Remote sensing ionospheric variations due to total solar eclipse, using GNSS observations

Mohamad Mahdi Alizadeh [a, b, *], Harald Schuh [b, c], Saeed Zare [a], Sahar Sobhkhiz-Miandehi [a], Lung-Chih Tsai [d, e]

[a] Dept. of Geodesy and Geomatics Eng., K. N. Toosi University of Technology, Tehran, Iran
[b] Inst. of Geodesy and Geoinformation Science, Technical University of Berlin, Berlin, Germany
[c] Dept. 1: Geodesy, GFZ German Research Center for Geosciences, Potsdam, Germany
[d] Center for Space and Remote Sensing Research, National Central University, Chung-Li, Taiwan, China
[e] GPS Application and Research Center, National Central University, Chung-Li, Taiwan, China

ARTICLE INFO

ABSTRACT

For years great interest has been taken in the effects of physical phenomena on ionosphere structure. A total solar eclipse was visible in North America on August 21st, 2017. This event offered a great opportunity for remote sensing the ionospheric behavior under the eclipse condition. In this study we investigated the effects of total solar eclipse on variations of Total Electron Content (TEC), and consequently deviations on regional models of Vertical TEC (VTEC), as well as variations in ionospheric scintillation occurrence. Although variations of TEC due to total solar eclipse are studied thoroughly by many authors, but the effect of solar eclipse on ionospheric scintillation has never been considered before. Our study is based on measurements from a high-rate GPS network over North America on the day of eclipse, a day before and after its occurrence, on the other hand, GPS measurements from ground-based stations on similar days were used to model TEC on the day of event, and also one day before and after it. The results of this study demonstrate that solar eclipse reduced scintillation occurrence at the totality region up to 28 percent and TEC values showed a decrease of maximum 7 TECU. Considering TEC models, our study showed apparent variations in the regional models, which confirms previous studies on ionospheric responses to eclipse as well as theoretical assumptions.

© 2019 Institute of Seismology, China Earthquake Administration, etc. Production and hosting by Elsevier B.V. on behalf of KeAi Communications Co., Ltd. This is an open access article under the CC BY-NC-ND license (http://creativecommons.org/licenses/by-nc-nd/4.0/).

1. Introduction

The ionosphere is the upper layer of the atmosphere and is produced when Sun's radiation ionizes atoms and molecules within this layer. According to ionospheric studies, solar radiation is the primary cause of the existence of this layer. As GPS signals travel through the ionosphere, this region of free electrons and ions inevitably affects them. Different natural and artificial phenomena affect the physical behavior of the Earth's ionosphere. Among these, the solar eclipse is a phenomenon, which has an apparent effect on the ionosphere. A solar eclipse occurs when Sun, Earth, and Moon are aligned at the phase of New Moon, in which the Moon is placed directly between the Sun and the Earth and its shadow falls on the Earth. Remote sensing the ionosphere during a solar eclipse provides great opportunity to study and investigate the effects of this phenomenon on ionospheric parameters and also ionospheric responses to solar eclipse over a short period of time. Ionosphere's plasma density irregularities may cause GPS signals to experience rapid amplitude and/or phase fluctuations, which are referred to as ionospheric scintillation [1]. The main reason for scintillation occurrence is related to ionosphere structure, which is highly correlated with solar radiation.

Many scientists have studied the effects of solar eclipses on the ionosphere, from which we can point out Ratcliffe [2], Davis et al.

* Corresponding author. Dept. of Geodesy and Geomatics Eng., K. N. Toosi University of Technology, Tehran, Iran.
E-mail address: alizadeh@kntu.ac.ir (M.M. Alizadeh).

[3], and Kovalev et al. [4] as the pioneers in this field. In 1968 Rishbeth [5] discussed the loss rate of ionization in the F region of ionosphere. Different methods have been used in order to detect ionospheric responses to eclipse, especially changes in Total Electron Content (TEC), such as using GPS-radio interferometry [6], or observing the Faraday rotation of polarization of lunar radio waves [7]. GPS observations were also used in many studies to analyze TEC changes due to the solar eclipse, e.g. Kumar [8], Jakowski [9] and Baran [10]. The ionospheric effects of a solar eclipse depend on several factors, such as latitude, longitude, local time and geophysical conditions, i.e. on each solar eclipse the geometry of eclipse formation, magnetizes plasma differently so none of them make exact similar disturbances [11]. After the American total solar eclipse occurrence in August 2017 studies have been done on Global Navigation Satellite System (GNSS) observation variations due to solar eclipse [12]. Ionospheric total electron response to the solar eclipse occurred in America was also studied by Cherniak & Zakharenkova [13].

In this study, we investigate the effects of the solar eclipse on ionospheric models and scintillation indices before, during, and after eclipse incidence at August 21st 2017 for each Pseudo Random Noise (PRN). Daily observations from more than 30 ground-based International GNSS Service (IGS) stations over North-America were used for ionosphere modeling and also high-rate GPS observations from a non-profit university-governed consortium (UNAVCO) data center which includes thousands of permanent stations distributed globally were used for studying scintillation indices. The obtained results of this study demonstrate that scintillation effects are significantly reduced when a solar eclipse occurs. Regarding TEC models, our results confirm previous studies on ionospheric responses to eclipse as well as theoretical assumptions.

2. Materials and methods

2.1. Calculating TEC from GNSS data

According to Limberger [14], the frequency dependent factors are summarized in

$$\alpha = 40.3 \frac{f_1^2 - f_2^2}{f_1^2 f_2^2} \tag{1}$$

where f_1 and f_2 are corresponding frequencies of phase measurements in L_1 and L_2 bands.

The geometry-free linear combination for code and phase measurements can be written as

$$P_{r,4}^s = P_{r,1}^s - P_{r,2}^s = -\alpha STEC_r^s + DCB + \varepsilon_{P_4} \tag{2}$$

$$L_{r,4}^s = \lambda_1 \Phi_{r,1}^s - \lambda_2 \Phi_{r,2}^s = \alpha STEC_r^s + CPB_{4,r}^s + \varepsilon_{L_4}, \tag{3}$$

where $STEC_r^s$ is Slant TEC between satellite s and receiver r, $P_{r,1}^s$ and $P_{r,2}^s$ are code measurements in L_1 and L_2 band, $\Phi_{r,1}^s$ and $\Phi_{r,2}^s$ are phase measurements in L_1 and L_2 band. The remaining unknowns in these equations are the bias terms for code and phase measurements. $DCB = c(\Delta b_r + \Delta b^s)$ is denoted as inter-frequency Differential Code Bias (DCB) and $CPB_{4,r}^s$ contains the merged carrier phase biases, in particular, the ambiguity differences $\lambda_1 N_1 - \lambda_2 N_2$. Following Schaer [15], the smoothed code $\overline{P_{r,4}^s}$ for both L_1 and L_2 frequencies is computed from

$$P_{r,4}^s = \begin{cases} \lambda_1 \Phi_{r,1}^s + \overline{P_{r,1}^s} - \overline{\lambda_1 \Phi_{r,1}^s} + \frac{2f_2^2}{f_1^2 - f_2^2}\left(L_{r,4}^s + \overline{\lambda_2 \Phi_{r,2}^s} - \overline{\lambda_1 \Phi_{r,1}^s}\right) & \text{for } f_1 \\ \\ \lambda_2 \Phi_{r,2}^s + \overline{P_{r,2}^s} - \overline{\lambda_2 \Phi_{r,2}^s} + \frac{2f_2^2}{f_1^2 - f_2^2}\left(L_{r,4}^s + \overline{\lambda_2 \Phi_{r,2}^s} - \overline{\lambda_1 \Phi_{r,1}^s}\right) & \text{for } f_2 \end{cases} \tag{4}$$

with $\overline{P_{r,1}^s}$ and $\overline{P_{r,2}^s}$ representing the mean code and $\overline{\lambda_1 \Phi_{r,1}^s}$ as well as $\overline{\lambda_2 \Phi_{r,2}^s}$ identifying the mean phase measurements referring to an uninterrupted data arc. It shall be noticed that the Differential Code Biases (DCBs) are still contained in the geometry-free observables $\widetilde{P_{r,4}^s}$ and $\widetilde{L_{r,4}^s}$.

It should also be mentioned that the accuracy of determining TEC depends on the accuracy of GPS observable used to extract TEC values. As we used smoothed code observable (Equation (4)), the accuracy depends on the carrier phase and code measurements obtained from each particular satellite to each individual station.

2.2. TEC modeling

In order to understand variations of the ionosphere due to the solar eclipse, parameters of the ionosphere, namely TEC are modeled before, during, and after the occurrence of the solar eclipse. In a two-dimensional approach, a spherical layer of infinitesimal thickness in which all electrons are concentrated often represents the ionosphere. The height of this idealized layer approximately is usually set to values between 350 and 450 kilometers [16]. Accordingly, Spherical TEC is transformed into the Vertical TEC (VTEC), which is spatially a two-dimensional function depending on longitude and latitude.

The most concrete and continuous results on GPS-based VTEC modeling are produced by the analysis centers of the IGS. Spherical harmonic base functions are the most widely used method in GPS-based global ionospheric modeling. Regional base functions such as B-splines can be used for regional models.

For regional modeling applications, we consider normalized quadratic polynomial B-splines denoted by $\Phi_k^{J_\phi}(x) = N_{k,m}^{J_\phi}(x)$ as one-dimensional basis function for representing the signal within a bounded interval (Schmidt, 2007). $N_{k,m}^{J_\phi}(x)$ are usual normalized B-splines of the order m with

$$\sum_{k=1}^{K_\phi} N_{k,m}^{J_\phi}(x) = 1 \quad x \in [0,1], \tag{5}$$

where $J_\Phi \in \mathbb{N}$ defines the B-spline resolution level and $k \in \{1,2,\ldots,K_\Phi\}$ identifies a specific spline function. The model resolution is controlled by the level J_Φ, i.e. the higher level, the finer the signal structures can be resolved. The basis for normalized quadratic polynomial B-splines is defined recursively [16,17] with

$$N_{k,1}^{J_\phi}(x) = \begin{cases} 1 & v_k^{J_\phi} \leq x \leq v_{k+1}^{J_\phi} \\ 0 & \text{otherwise} \end{cases}, \quad k = m, \ldots, K_\phi \tag{6}$$

$$N_{k,m}^{J_\phi}(x) = \frac{x - v_k^{J_\phi}}{v_{k+m-1}^{J_\phi} - v_k^{J_\phi}} N_{k,m-1}^{J_\phi}(x) \\ + \frac{v_{k+m}^{J_\phi} - x}{v_{k+m}^{J_\phi} - v_{k+1}^{J_\phi}} N_{k+1,m-1}^{J_\phi}(x), \quad m \geq 2. \tag{7}$$

The regional 2D representation of VTEC by means of tensor products of two linearly independent 1-D B-spline functions can be expressed as

$$VTEC(\varphi, \lambda, t_i)_R = \sum_{k_1=1}^{K_1} \sum_{k_2=1}^{K_2} d_{k_1,k_2}^{J_1,J_2}(t_i) \phi_{k_1}^{J_1}(\varphi) \phi_{k_2}^{J_2}(\lambda) \tag{8}$$

where φ indicates the geographic or geomagnetic latitude and λ the geographic or sun-fixed longitude. A subscript R has been introduced to indicate the regional model space. Equation (8) refers to astatic representation of the epoch t_i. For more details on B-spline modeling refer to [18].

2.3. Scintillation detection

As a radio wave passes through the ionosphere it might meet a region of irregularities and then sudden signal phase and amplitude variations may appear. These variations caused by small ionospheric irregularities are referred to as scintillation and are divided into two categories. Amplitude scintillation, which refers to rapid fluctuations in signal intensity, and phase scintillation, which is related to rapid fluctuations in carrier-phase measurements. Ionospheric scintillation which can cause signal fades is considered as a spatial phenomenon with a scale length called the Fresnel length calculated by $\sqrt{2\lambda d}$, where λ is the signal wavelength and d is the distance from receiver to the region in which scintillation has occurred [19].

Since scintillation occurrence directly affects GPS signals, studying GPS observations is a common and appropriate way for its detection. Many indices are used to investigate ionospheric activity and its characteristics. One of the most common indices among them is the S4 index, which is essentially used to detect small scale irregularities and rapid variations of the ionospheric structure. It is called scintillation and is calculated by the use of GPS signal intensities driven from GPS receiver outputs. S4 that is actually defined as variance of normalized signal intensity from receiver's output data [20] can be calculated as

$$S4 = \sqrt{\frac{\overline{S_i^2} - \overline{S_i}^2}{\overline{S_i}^2}} \tag{9}$$

where S_i denotes the signal intensity driven from GPS output and bar sign is average of data on a period of time that depends on the time scale of interest. In this study, S4 values have been calculated every 1-minute which is more common. According to previous studies [21] when S4 amount is between 0.2 and 0.4 it is called weak scintillation, S4 values between 0.4 and 0.6 show middle scintillation, and if the value is higher than 0.6 the scintillation is strong [22].

3. Data

This study is based on GPS measurements from more than 40 IGS stations and 20 stations of UNAVCO. UNAVCO is a non-profit university-governed consortium that facilitates geoscience research and education using Geodesy. UNAVCO website (http://www.unavco.org/) provides free 1, 2, 5 and 10 HZ GPS observation data in RINEX format. Fig. 1 is a globe view of the eclipse path derived from National Aeronautics and Space Administration (NASA) website and Fig. 2 shows a network of stations used in this study and the totality path of solar eclipse occurred on August 21st, 2017.

In order to show the variations of TEC around the eclipse hours, observations from IGS stations were used. One of them is located in

Colorado Springs, which is approximately 450 km far from eclipse's path of totality, and the other one, which is located in North Liberty which is about 350 km far from totality path. Both experience a partial eclipse with more than 80% of obscuration. Table 1 shows the exact location of the two stations.

For studying ionospheric scintillation over the period of total eclipse, S4 index was calculated at two stations with 1 Hz sampling rate from UNAVCO network. All of them experienced a partial eclipse with almost 50% obscuration. Table 2 provides more detailed information of these stations.

4. Results

4.1. Variations in TEC value

In order to study solar eclipse effects on TEC variations two approaches were considered: diurnal TEC variations and variations in regional TEC model. In the first approach, single site technique was used to study diurnal variations of TEC. IGS stations in the region close to the solar eclipse were selected and temporal variations of TEC on a day before, during, and after solar eclipse were studied. GPS measurements from all satellites observed at stations (see Table 1) during a 24-hour time period were taken into account.

Fig. 3 presents the diurnal TEC variations over NLIB and AMC2 stations on 20th, 21st, and 22nd August 2017. The arrow on Fig. 3(b) points out the time of maximum phase of the solar eclipse over the stations. Time series of TEC values on the day before, during, and after the solar eclipse provides a good basis to study the effect of the solar eclipse on TEC variations. The mean values of TEC on the day of eclipse are lower comparing to the other days. As it can be seen from Fig. 3(b), the eclipse effect occurs as trough-like of depression. Around the maximum phase of the eclipse for each station the TEC values reach their minimum. The minimum level of TEC persists around 30—60 min, and then it slowly recovers for the next 3—4 h. As seen in Fig. 3, the time of maximum effect is different for each station, which is related to their location. At NLIB station the depression of TEC is about 3 TECU and for Colorado Springs (AMC2) this amounts to about 7 TECU. This depression can be seen in other
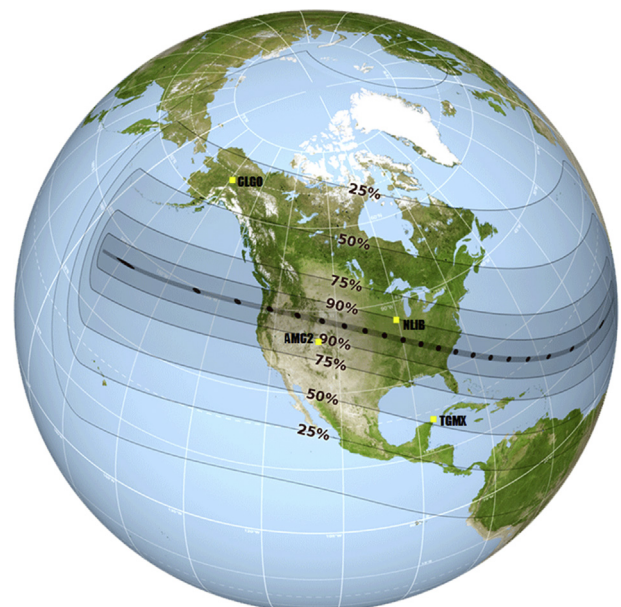

Fig. 1. A globe view of the eclipse path [23]. The four main stations of this study are indicated on the map.
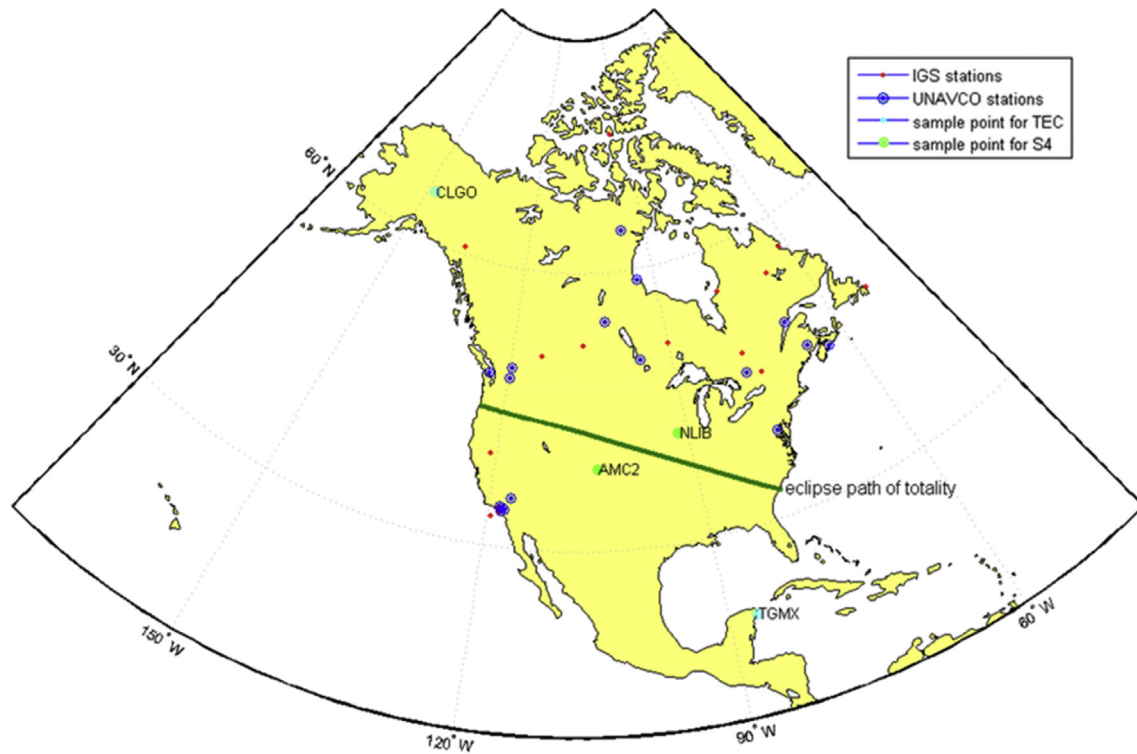
Fig. 2. A map of stations around eclipse's path of totality that have been used.

Table 1
Station information for TEC measurements.

Station	Longitude	Latitude	Start of partial eclipse (UT)	End of partial eclipse (UT)
AMC2, Colorado Springs	−104.52°	38.80°	16:23	19:16
NLIB, North Liberty	−91.57°	41.77°	16:47	19:37

Table 2
Station information for scintillation detection.

Station	Longitude	Latitude	Start of partial eclipse (UT)	End of partial eclipse (UT)
CLGO, Fairbanks	−147.86°	64.87°	16:29	18:16
TGMX, Quintana Roo	−86.87°	20.88°	17:22	20:13

IGS stations and the solar eclipse effect is weaker if the distance of the station and pass of totality is longer.

For the detailed analysis of TEC response to the eclipse, we studied the variation of absolute TEC along a single satellite pass. During the eclipse occurrence over NLIB station several satellites were observed, i.e. PRN 2, PRN 6, PRN 12, PRN 17, and PRN 19. Variations of TEC derived from phase measurements for a day before, during, and after the solar eclipse along satellite passes at NLIB station are presented in Fig. 4.

The behavior of TEC at other stations is similar to NLIB. As it can be seen, during the solar eclipse the TEC depression around 18 Universal Time (UT) is recognized for all satellites (Fig. 4 – column (b)). The time of minimum value of TEC with respect to the maximum phase of the eclipse varies in each station and the level of TEC depression is different for each individual satellite.

4.2. Variations in TEC models

For analysis of spatial distribution of the TEC in the region of interest during the solar eclipse, regional TEC models were derived by the use of regional base functions. For regional modeling of TEC, we used GPS measurements collected at around 40 IGS stations using pseudo-range code and phase measurements. TEC maps were produced with 1-hour interval, by using normalized quadratic polynomial B-splines. For comparison, global VTEC values extracted from the Global Ionosphere Maps (GIM) obtained from the IGS were used. These maps, downloaded from the Crustal Dynamics Data Information System (CDDIS) ftp site [24], provide thirteen two-hourly maps at each of the three days of 20th, 21st, and 22nd August 2017. The maps of VTEC over the region of the total solar eclipse at 18 Coordinated Universal Time (UTC) are presented in Fig. 5. For comparison, regional and global TEC maps are depicted in three respective days, i.e. a day before, during, and a day after solar eclipse of 21st August 2017.

In order to better understand the maps of Fig. 5, Fig. 6 depicts the VTEC map differences between the day of the solar eclipse and the days before and after solar eclipse occurrence. As it can be seen, this difference can reach up to 7 TECU in specific areas. These differences are recognizable in both regional and global maps. Of course, more details are apparent in regional maps.
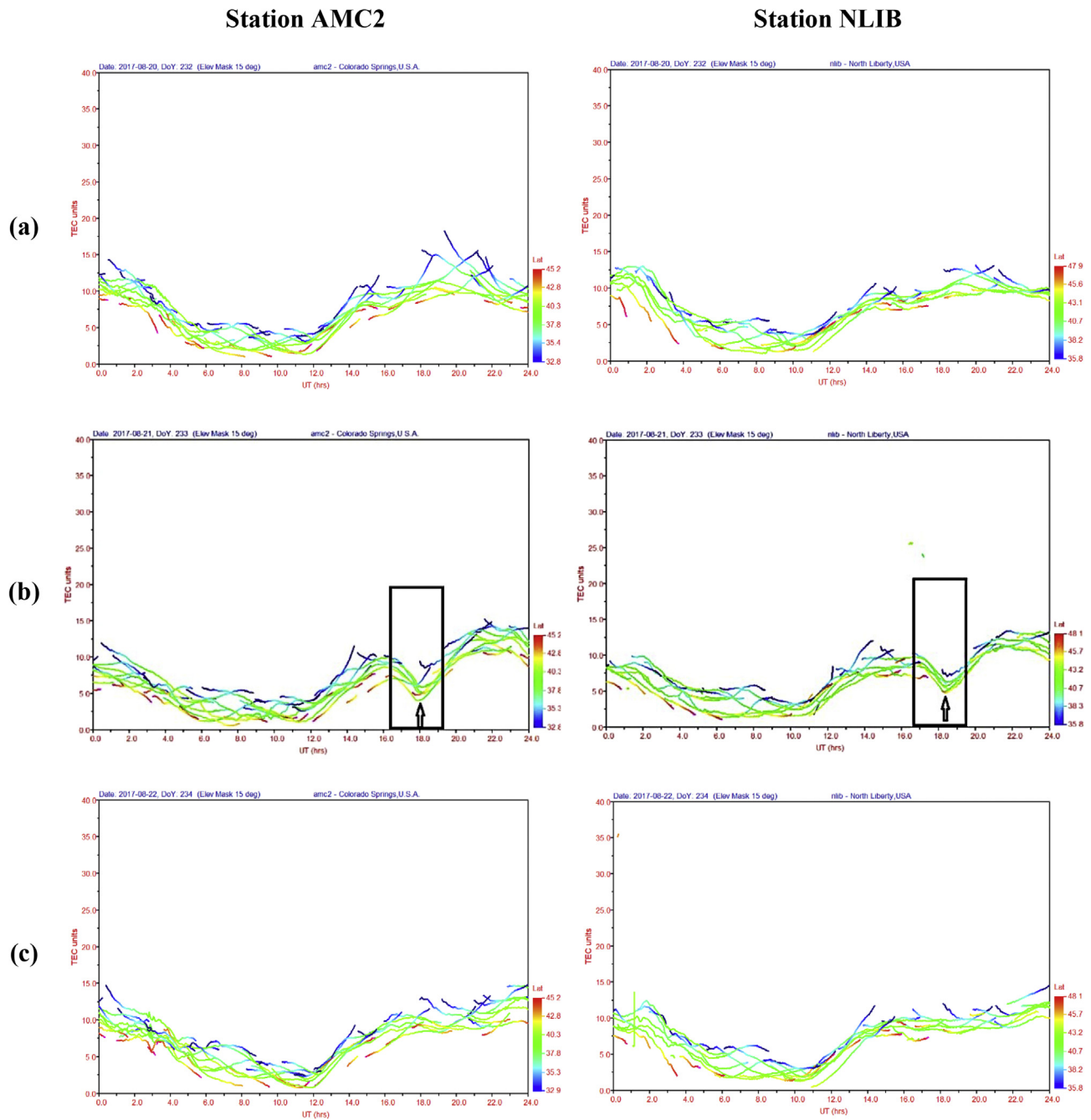
Station AMC2   ## Station NLIB

Fig. 3. Diurnal variations of TEC at AMC2 station (left column) and NLIB station (right column) on (a) 20th, (b) 21st, and (c) 22nd August 2017. The arrow shows the maximum phase of the solar eclipse at the stations. (The eclipse hours has been shown by the black box in column (b)).

4.3. Variations in ionospheric scintillation occurrence

Regarding scintillation occurrence during the total solar eclipse, a decrease of up to 30 percent is evident in the region of study. Considering the latitude in which the solar eclipse has occurred, the probability of ionospheric scintillation occurrence is very low. But despite the fact that the total solar eclipse has occurred in a very quiet area in terms of scintillation detection, some amount of S4 index reduction has been indicated by our results.

The calculated S4 values were all under 0.2, which means there is no scintillation influence on GPS signals. Fig. 7 shows diurnal variations of S4 values calculated for two stations mentioned in Table 2 for August 20th, 21st, and 22nd. As it can be seen there is a very small reduction in S4 values at August 21st in the eclipse hours.

It is worth mentioning that due to the high correlation between the index of geomagnetic activity (Kp index) and ionospheric scintillation occurrence, this index has been considered over 3 days of our study via GFZ-Potsdam Kp index ftp-site [25]. The Kp index on August 20th, 21st, and 22nd at the eclipse hours were 3, 2 and 2 respectively. None of these index values indicate signs of active geomagnetic hours.
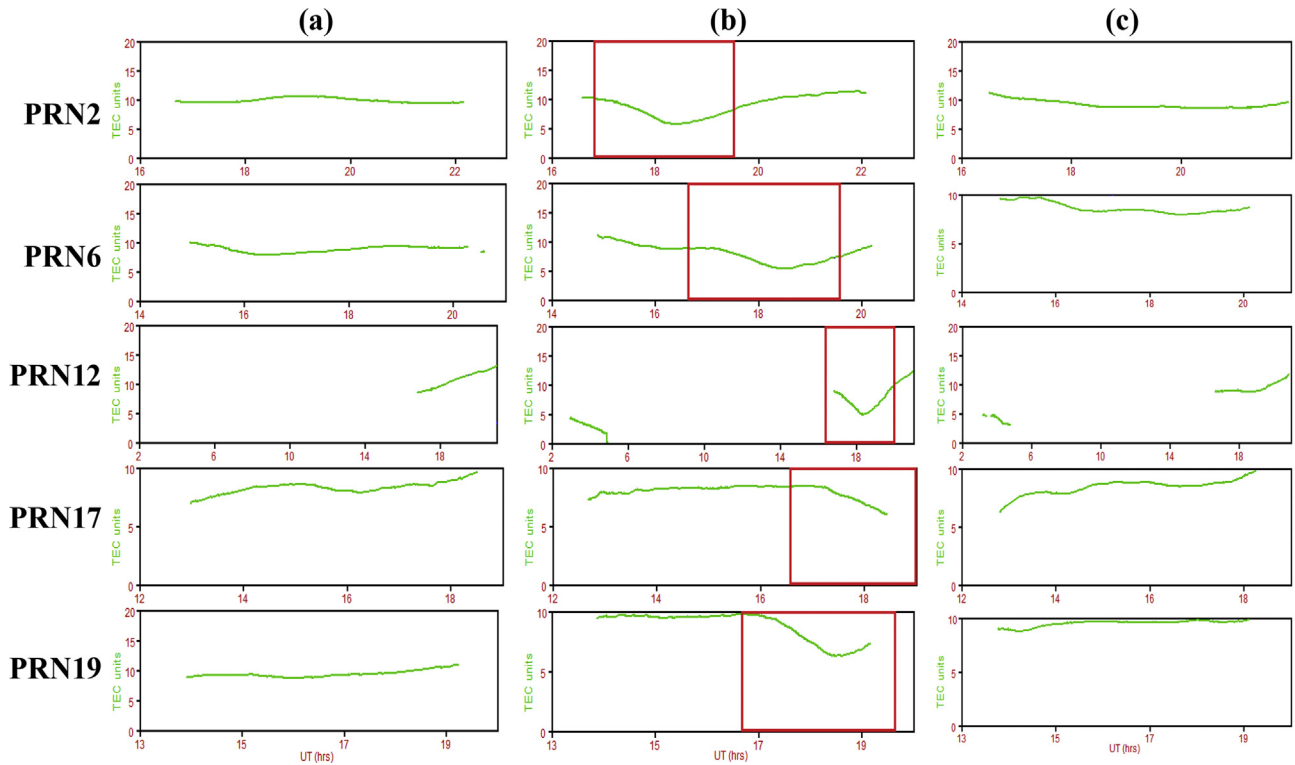
Fig. 4. Variations of TEC along satellite passes (PRN 2, 6, 12, 17, and 19 rows respective) for NLIB station during (a) a day before, (b) during, and (c) a day after solar eclipse of 21st August 2017. (The red box highlights the eclipse hours).
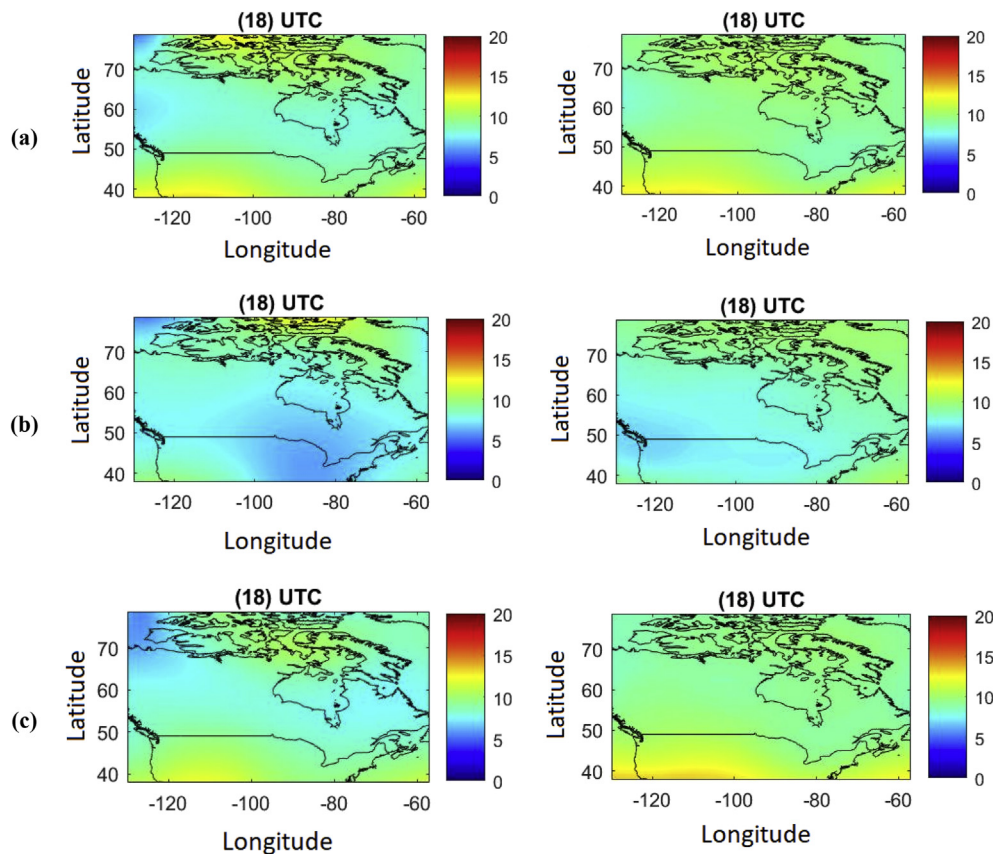

Fig. 5. The regional TEC maps (left column) and GIMs (right column) for the days August 20th, 21st, and 22nd 2017 (Rows, respectively).
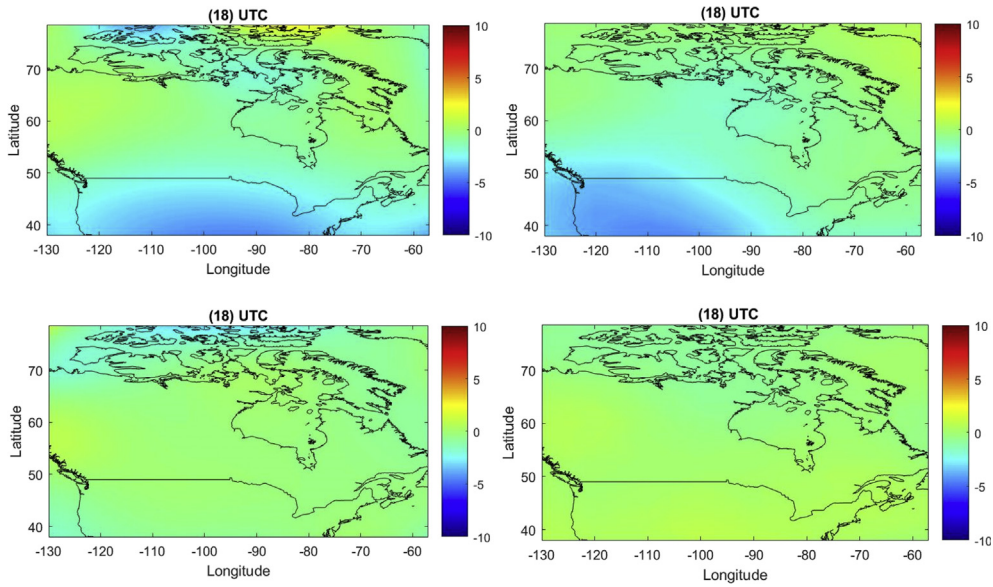
Fig. 6. TEC difference maps between 21st and 20th August (first row) and between 20th and 22nd August (second row) as references days in two case of regional (left column) and GIM (right column).
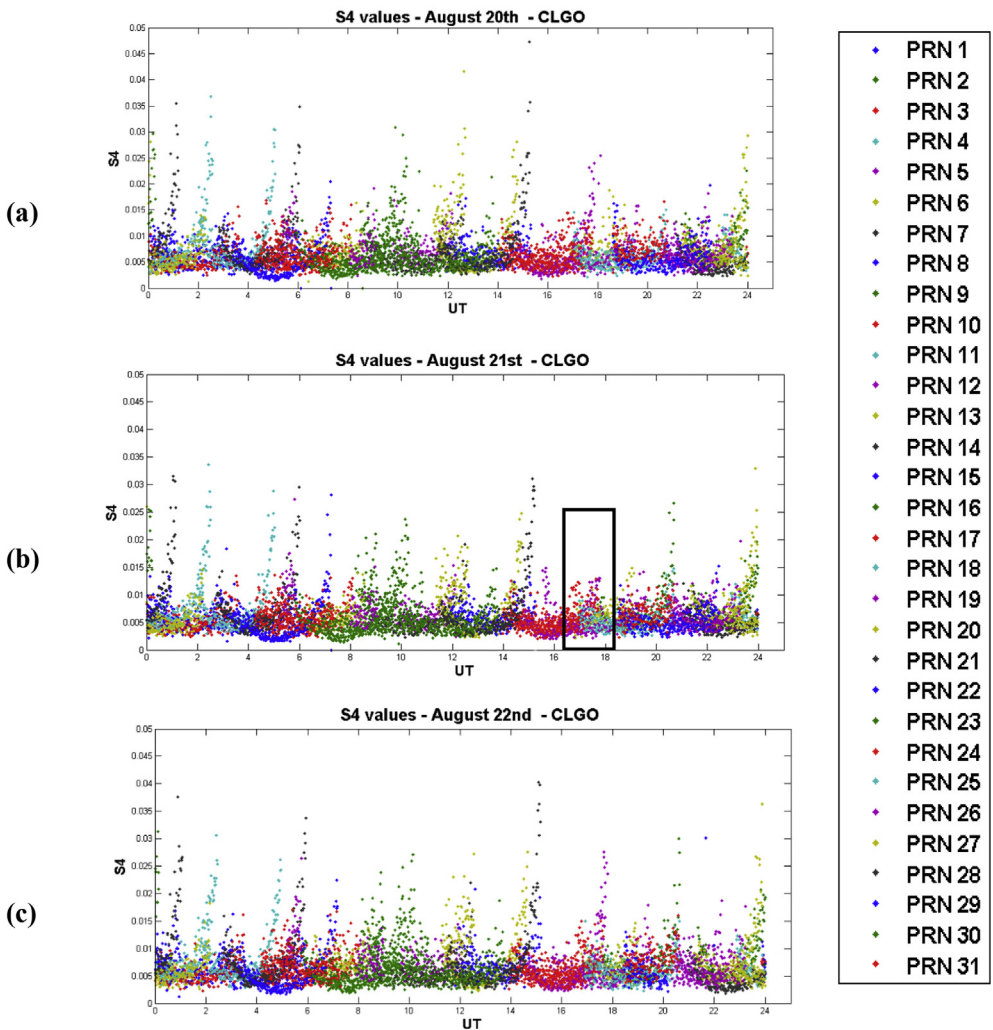

Fig. 7. Diurnal variations of S4 values in CLGO station for (a) one day before eclipse (b) at the day of solar eclipse occurrence and (c) one day after the event. (The eclipse hours have been shown by the black box).

In order to obtain most reliable results of determining the parameters of the ionosphere and to avoid multi-path effects, a 30-degree cut-off angle for each path has been considered.

As it can be seen in both Figs. 7 and 8, S4 values show a slight reduction during the occurrence of total solar eclipse, i.e. on 21st of August from around 16:00 until after 18:00 UT at the station CLGO, and from around 18:00 until after 20:00 UT at station TGMX.

Comparing the S4 values of station CLGO during the total solar eclipse hours (values within the black box in Fig. 7(b)) with similar time at a day before and a day after the total solar eclipse shows a reduction of around 18.7%. Similar comparison at station TGMX (values within the black box in Fig. 8(b)) shows a reduction of 28.9% in the S4 values. Since the S4 values are directly related to the occurrence of ionospheric scintillation, it can be concluded that the occurrence of ionospheric scintillation is reduced in both stations during the occurrence of total solar eclipse. Although comparing the two stations with each other, this reduction is more in TGMX than in CLGO. This can be due to the fact that station TGMX is in lower latitude, comparing to station CLGO, and the occurrence of ionospheric scintillation in lower latitudes is more probable.

5. Conclusions

At August 21st, 2017 a total solar eclipse was visible in North America, which offered a great opportunity to study ionospheric behavior under eclipse condition. In this study, GPS observations over North America on the day of eclipse, one day before and one day after its occurrence were processed to investigate ionospheric responses to this event.

Variations in TEC, variations in the regional and global models of VTEC, and variations in the S4 value, which indicates the variation in the occurrence of ionospheric scintillation, were studied during the occurrence of total solar eclipse. Although the first two parameters were thoroughly investigated by several authors, studying ionospheric scintillation due to solar eclipse was investigated for the first time.

Regarding TEC values, the results at different stations and for each signal path from a satellite to a receiver showed a reduction between 3 and 7 TECU during the occurrence of total solar eclipse, which confirms previous studies and theoretical assumptions.
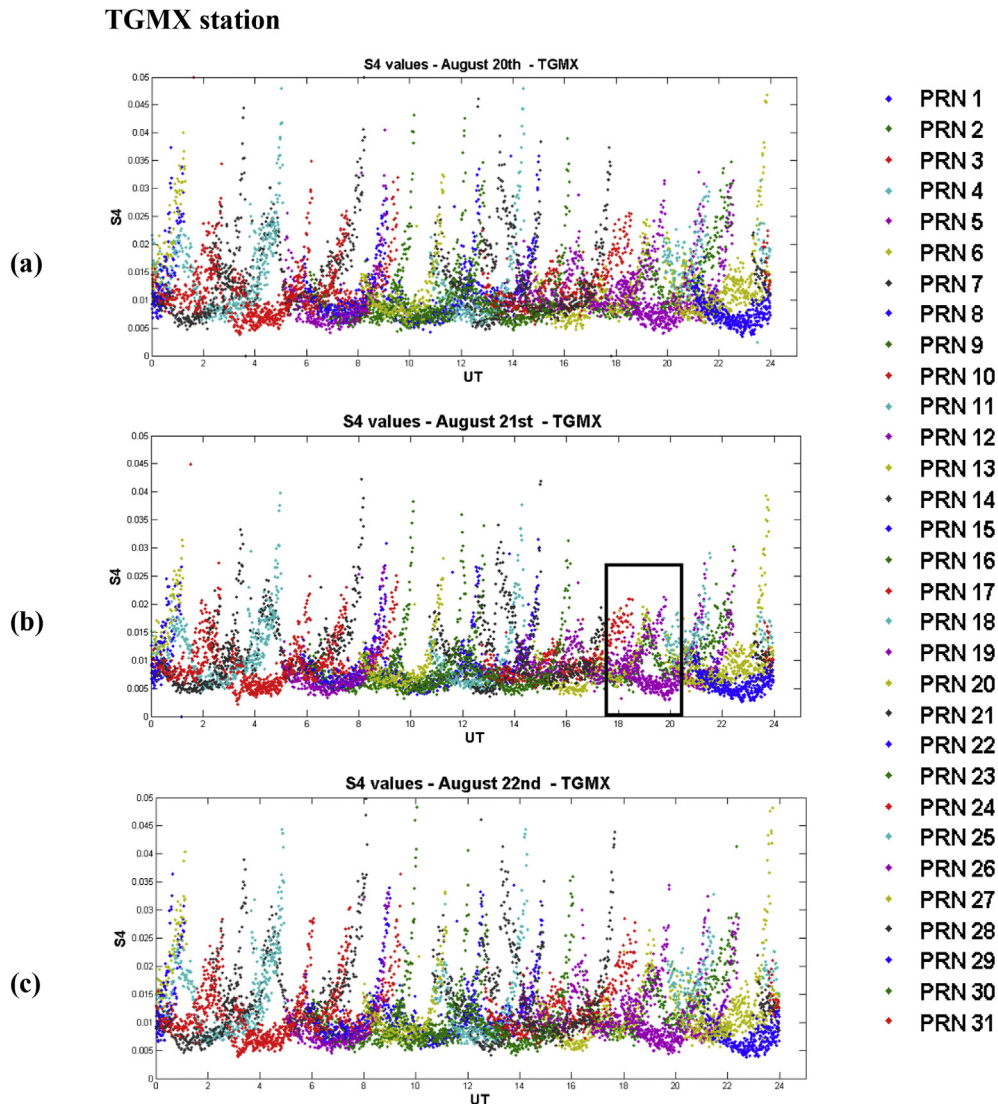

Fig. 8. Diurnal variations of S4 values in TGMX station for (a) one day before eclipse (b) at the day of solar eclipse occurrence and (c) one day after the event. (The eclipse hours have been shown by the black box).

Regarding VTEC maps, the occurrence of total solar eclipse had a clear effect on both global and regional maps. The difference in the VTEC map of the day of total solar eclipse and the maps of one day before and one day after the occurrence revealed a maximum difference of up to 7 TECU. Of course more details were apparent in regional maps comparing to global maps.

Finally, scintillation occurrence was studied for the first time during total solar eclipse. For this S4 values at different stations were studied during the day of total solar eclipse occurrence, a day before, and a day after the occurrence. The studies revealed that the occurrence of total solar eclipse has effects on reducing the S4 values, and consequently in reducing the probability of ionospheric scintillation occurrence. The results showed a reduction of about 18—29% in the S4 values depending on the location of the station being studied.

Conflicts of interest

The authors declare no conflict of interest.

Acknowledgments

Abbreviations

DCB Differential Code Bias
GIM Global Ionosphere Map
GNSS Global Navigation Satellite Systems
GPS Global Positioning System
IGS International GNSS Service (IGS)
PRN Pseudo Random Noise
TEC Total Electron Content
TECU Total Electron Content Unit
UT Universal Time
VTEC Vertical Total Electron Content

References

[1] R.S. Conker, M.B. El-Arini, C.J. Hegarty, T. Hsiao, Modeling the effects of ionospheric scintillation on GPS/Satellite-Based Augmentation System availability, Radio Sci. 38 (1) (2003) 1001.
[2] J. Ratcliffe, A survey of solar eclipses and the ionosphere. Solar Eclipses and the Ionosphere, J. Atmos. Terr. Phys. 6 (Special suppl) (1956) 1—13.
[3] C.J. Davis, E.M. Clarke, R.A. Bamford, M. Lockwood, S.A. Bell, Long term changes in EUV and X-ray emissions from the solar corona and chromosphere as measured by the response of the Earth's ionosphere during total solar eclipses from 1932 to 1999, Ann. Geophys. 19 (3) (2001) 263—273.
[4] A.A. Kovalev, A.G. Kolesnik, S.A. Kolesnik, A.A. Kolmakov, R.R. Latypov, Ionospheric effects of solar eclipses at midlatitudes, Geomagn. Aeron. 49 (4) (2009) 476—482.
[5] H. Rishbeth, Solar eclipses and ionospheric theory, Space Sci. Rev. 8 (4) (1968) 543—554.
[6] E. Afraimovich, K. Palamartchouk, N. Perevalova, V. Chernukhov, A. Lukhnev, V. Zalutsky, Ionospheric effects of the solar eclipse of March 9, 1997, as deduced from GPS data, Geophys. Res. Lett. 25 (4) (1998) 465—468.
[7] J.A. Klobuchar, H. Whitney, Ionospheric electron content measurements during a solar eclipse, J. Geophys. Res. 70 (5) (1965) 1254—1257.
[8] S. Kumar, A. Singh, R. Singh, Ionospheric response to total solar eclipse of 22 July 2009 in different Indian regions, Ann. Geophys. 31 (2013) 1549—1558.
[9] N. Jakowski, S.M. Stankov, V. Wilken, C. Borries, D. Altadill, J. Chum, D. Buresova, J. Boska, P. Sauli, F. Hruska, Ionospheric behavior over Europe during the solar eclipse of 3 October 2005, J. Atmos. Sol. Terr. Phys. 70 (6) (2008) 836—853.
[10] L. Baran, I. Ephishov, I. Shagimuratov, V. Ivanov, A. Lagovsky, The response of the ionospheric total electron content to the solar eclipse on August 11, 1999, Adv. Space Res. 31 (4) (2003) 989—994.
[11] T. Farges, J. Jodogne, R. Bamford, Y. Le Roux, F. Gauthier, P. Vila, D. Altadill, J. Sole, G. Miro, Disturbances of the western European ionosphere during the total solar eclipse of 11 August 1999 measured by a wide ionosonde and radar network, J. Atmos. Sol. Terr. Phys. 63 (9) (2001) 915—924.
[12] A.J. Coster, L. Goncharenko, S.R. Zhang, P.J. Erickson, W. Rideout, J. Vierinen, GNSS observations of ionospheric variations during the 21 August 2017 solar eclipse, Geophys. Res. Lett. 44 (24) (2017), 12,041-112,048.
[13] I. Cherniak, I. Zakharenkova, Ionospheric total electron content response to the great American solar eclipse of 21 August 2017, Geophys. Res. Lett. 45 (3) (2018) 1199—1208.
[14] M. Limberger, Ionospheric Modeling from GPS Radion Occultations and Complementary Data Based on B-Splines, Phd Thesis, Universitätsbibliothek der TU München, Germany, 2015. ISBN 978-3-7696-5167-6.
[15] S. Schaer, Mapping and Predicting the Earth's Ionosphere Using the Global Positioning System 59, Institut für Geodäsie und Photogrammetrie, Eidg. Technische Hochschule Zürich, 1999.
[16] L.L. Schumaker, C. Traas, Fitting scattered data on spherelike surfaces using tensor products of trigonometric and polynomial splines, Numer. Math. 60 (1) (1991) 133—144.
[17] E.J. Stollnitz, A.D. DeRose, D.H. Salesin, Wavelets for computer graphics: a primer. 1, IEEE Comput. Graph. Appl. 15 (3) (1995) 76—84.
[18] M. Schmidt, Wavelet modelling in support of IRI, Adv. Space Res. 39 (5) (2007) 932—940.
[19] Y. Jiao, Y. Morton, S. Taylor, Comparative studies of high-latitude and equatorial ionospheric scintillation characteristics of GPS signals, in: 2014 IEEE/ION Position, Location and Navigation Symposium-PLANS, 2014, pp. 37—42, https://doi.org/10.1109/PLANS.2014.6851355.
[20] L. Pan, P. Yin, Analysis of polar ionospheric scintillation characteristics based on GPS data, in: China Satellite Navigation Conference (CSNC) 2014 Proceedings, 2014, https://doi.org/10.1007/978-3-642-54737-9_2.
[21] B. Xiong, W.X. Wan, B.Q. Ning, H. Yuan, G.Z. Li, A comparison and analysis of the S4 index, C/N and Roti over Sanya, Chin. J. Geophys. 50 (6) (2007) 1414—1424.
[22] S. Basu, K. Groves, J. Quinn, P. Doherty, A comparison of TEC fluctuations and scintillations at Ascension Island, J. Atmos. Sol. Terr. Phys. 61 (16) (1999) 1219—1226.
[23] NASA Eclipse Data website: https://eclipse2017.nasa.gov.
[24] CDDIS ftp site: https://ftp.cddis.eosdis.nasa.gov/.
[25] GFZ-Potsdam Kp index ftp-site: https://www.gfz-potsdam.de/en/kp-index/.

Mohamad Mahdi Alizadeh got his Ph.D. in Geodesy from Vienna University of Technology in 2013. Thereafter he spent about three years as a post-doc fellow at the Technical University of Berlin. He pursued his career as an assistant professor at K. N. Toosi University of Technology in Iran since 2016. His research is mainly focused on atmospheric studies, including ionospheric modeling, ionospheric irregularities and vertical coupling of ionosphere/ troposphere, using various space geodetic techniques.

Harald Schuh is the Director of Department 1 "Geodesy" at GFZ German Research Centre for Geosciences in Potsdam, Germany, and professor for "Satellite Geodesy" at the Technical University of Berlin. He has engaged in space geodetic research for more than 35 years with special focus on tropospheric and ionospheric modeling, VLBI (Very Long Baseline Interferometry), and earth rotation.

Saeed Zare got his Master of Science degree in 2018 from K. N. Toosi University of Technology in Iran. His studies focused mainly on modeling electron density by combining different satellite geodetic techniques.

Sahar Sobhkhiz got her Master of Science degree in 2018 from K. N. Toosi University of Technology in Iran. Her studies focused mainly on ionospheric scintillation detection using GNSS.

Lung-Chih Tsai is a professor at the National Central University in Taiwan, China. His research focuses on the study of the ionosphere and upper atmosphere: theory and instrument of ionospheric sounders, data processing and analysis to GPS receiver and radio occultation system, satellite beacon receiver, and JASON.